Chalcogenide Letters Vol. 20, No. 8, August 2023, p. 619 - 628

Structural, electronic, elastic, and optical properties of chalcogenide perovskite $SrZrS_3$ under ambient and high-pressure conditions

M. L. Han*, Y. Hu
Shaanxi College of Communications Technology, Shaanxi, 710018, China

Hydrostatic pressure is an effective tool that can give rise to novel crystal structures and physical properties. In this paper, we perform the first-principles calculation based on density-functional theory (DFT) to study the structural, electronic, elastic, and optical properties of chalcogenide perovskite $SrZrS_3$ under pressure. The results indicated that both the lattice constant and cell volume decrease with the increase of pressure, which are matched well with available previous values. The obtained elastic constants reveal the $SrZrS_3$ is mechanically stable between 0 and 15 GPa. Additionally, the main features of the valence and conduction bands have been analyzed from the total and partial density of states. The complex dielectric function, refractive index, absorption coefficient, reflectivity, and the extinction coefficient are also calculated and analyzed. According to our work, we found that the optical properties of $SrZrS_3$ undergo a red shift with increasing pressure.

(Received March 23, 2023; August 31, 2023)

Keywords: Chalcogenide perovskite, Electronic properties, Density functional theory

1. Introduction

Chalcogenide perovskites containing group-VI anions including S and Se are emerging as a novel class of semiconductors with potential photovoltaic and optoelectronic applications[1-3]. Due to their ferroelectric, piezoelectric, electrolytic, and optoelectronic properties enabling many advances in applications, chalcogenide perovskites have attracted significant attention[4]. Compared to lead halide perovskites, chalcogenide perovskites materials are more environmentally friendly and possess superior electronic and optical properties, suggesting their potential ideal for low-cost tandem solar cell application. Thus, it timely to predict the behavior of this material under different pressures by use of theoretical research and analysis.

As we know, fundamental physical properties are governed primarily by crystal structures, high expectation exists for chalcogenide perovskites. In perovskites of the type ABX_3, the BX_6 octahedron has been found to be the main decisive factor leading to desirable photovoltaic properties[5]. From a fundamental point of view, the corner-shared octahedrons in these chalcogenide perovskites such as $SrZrS_3$, give rise to less localized band minima and carriers with higher mobility, which proving to be more applicable for photovoltaic applications[6]. Previous theoretical studies by Oumertem *et al.* have characterized the electronic and thermodynamic properties of the cubic and

* Corresponding author: hanmeilin202303@126.com
https://doi.org/10.15251/CL.2023.208.619

orthorhombic $XZrS_3$ (X = Ba, Sr, Ca) compounds, predicting their band gap in the range of 1.15-1.62 eV[7]. Thermal stability investigations by Niu *et al.* on synthesized $SrZrS_3$ and $BaZrS_3$ show that these chalcogenide perovskites possess excellent thermal stability in air for a temperature range up to 550 °C[8]. Ju *et al*. predicted a series of chalcogenide perovskites such as $SrSnSe_3$, $CaSnS_3$ and $SrSnS_3$ with tunable direct bandgaps within the optimal range of 0.9-1.6 eV for single junction solar cell applications[9]. Recent investigation shows that the optical transitions near the band edges of chalcogenide perovskites differ from those of their halide counterparts[10]. Moreover, it is well known that high pressure plays an important character in the mechanical, elastic, optical and electronic properties of material performances. High pressure processed chalcogenide perovskite materials have obtained many exhilarating results such as photo-response enhancement, structural stability enhancement, bandgap optimization[11-12]. So, in this work, we have performed a comprehensive study on the structural, mechanical, and electronic properties of the $SrZrS_3$ perovskite as a function of pressure using first-principles calculations based on density functional theory (DFT). The information of lattice parameters, band structure, total density of states (DOS) and partial density of states (PDOS) under pressure are provided. Meanwhile, the values of mechanical parameters, such as the elastic constant, and elastic moduli are also calculated.

2. Computational methods

Calculations were performed using density functional theory (DFT) within the Perdew-Burke-Ernzerhof (PBE) generalized gradient approximation (GGA) as implemented in the Vienna ab initio simulation package (VASP)[13-15]. The all-electron projector augmented wave (PAW) method was adopted for Sr, Zr, and S atoms with valence electrons of $4s^24p^65s^2$, $4s^24p^64d^25s^2$, and $3s^23p^4$, respectively. The self-consistent calculations were carried out with a 7×6×7 k-point mesh[16]. All the structures were compressed from 0 to 15 GPa and at every studied pressure point, the structures were relaxed. The initial existing structure was taken at ambient pressure and the volume was reduced subsequently to achieve high pressures. To balance accuracy and speed, the plane-wave basis set cutoff was set to 750 eV. The convergence criteria for total energy, max force, max tress, and SCF iterations were 5×10^{-6}eV/atom, 0.01eV/Å, 0.02 GPa, and 5×10^{-7}eV/atom, respectively.

3. Results and discussion

3.1 Structural properties

To optimize the lattice constants at different pressures, we used the experimental lattice parameters and atomics positions as starting point for full structural optimization. The optimized lattice constants as functions of pressure are listed in Table 1 and depicted in Fig. 1. The predicted lattice constants of $SrZrS_3$ are *a*=7.162 Å, *b*=9.823 Å, and c = 6.771 Å, respectively, consistent with experimental findings[17]: *a*=7.125 Å, *b*=9.772 Å, and c = 6.748 Å, (Table 1), as well as previous other theoretical results[18]. It can also be observed that our theoretical *a*, *b*, and *c* values are very close to our experimental results (difference below 2%), which implying that the theoretical level we used in the calculations are accurate for predicting the structure properties of $SrZrS_3$.

Table 1. Calculated zero-pressure lattice constants (a, b, c) (Å), crystal cell volume V (Å³) of orthorhombic $SrZrS_3$ compound, together with the experimental and other theoretical data.

Method	a (Å)	b (Å)	c (Å)	V(Å³)
GGA	7.162	9.823	6.771	477.65
[17]Exp.	7.125	9.772	6.748	----
[18]Cal.	7.109	9.766	6.735	472.78

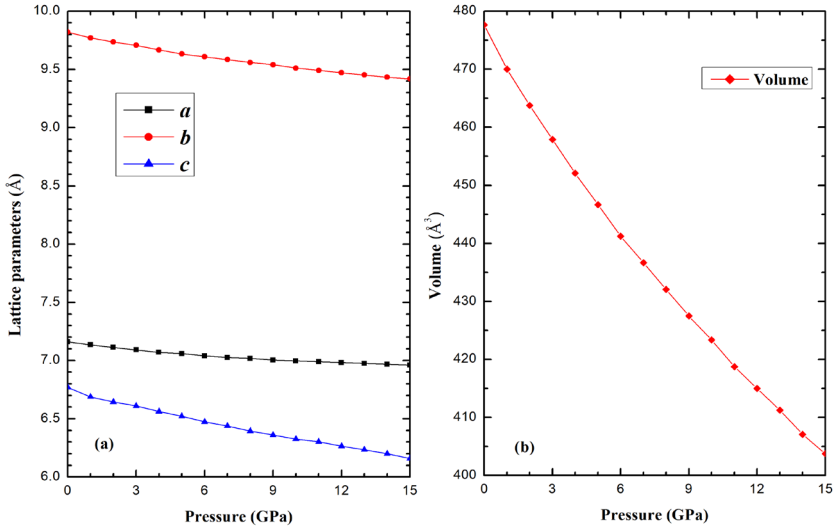

Fig. 1. The lattice parameters of the orthorhombic $SrZrS_3$ under high pressure up to 15 GPa.

Furthermore, by increasing the applied pressure from 0 to 15 GPa, the lattice constants *a*, *b*, and *c* decrease slightly from 7.162 to 6.961 Å, 9.823 to 9.419 Å, and from 6.771 to 6.158 Å, respectively. One can see that the lattice constants *a, b* and *c* decreased consistently with pressure. From a theoretical point of view, as the pressure increases, the interaction between Sr, Zr and S atoms becomes stronger and therefore the bond length among these atoms becomes shorter as a result the lattice parameters become smaller with pressure. At 15 GPa, the lattice parameter *a*, *b*, and *c* of orthorhombic $SrZrS_3$ are reduced by 2.8%, 4.1%, and 9.1%, respectively, which indicates that the crystal structure is compressed under pressure, and the lattice parameter gradually decreases as the external pressure increases, resulting in a gradual decrease in the unit cell volume. This similar behavior was often observed in chalcopyrite compound such as $SrMS_3$ (M=Ti and Nb), and $BaZrS_3$[19-20].

Meanwhile, the obtained pressure-unit cell volume (P-V) data set was used to obtain the Bulk modulus B_0 and its pressure derivative B_0' by fitting the data to the Birch-Murnaghan equation of state (EOS)[21] (Fig. 1(b)) along with the experimental data. At 15 GPa, the volume compression is V/V_0=84.53%, (V=403.75 $Å^3$, V_0=477.65 $Å^3$). The pressure derivative of bulk modulus is a parameter of great physical significant in high pressure physics. The obtained parameters for the bulk modulus and its first pressure derivative at ambient pressure and temperature

is B_0 =66.12 GPa and its derivative is $B'_0 = 3.97$, respectively, which are found to yield similar results in the pressure range for the theoretical data of B_0 =65.67 GPa and $B'_0 = 4$[18]. These results are expected to provide useful guidance for the structural characterization of this material under high pressure.

3.2. Elastic properties

It is well established that first-principles studies based on DFT can be used to obtain reliable elastic properties of inorganic compounds. Elastic constants are defined by means of a Taylor expansion of the total energy, the energy of a strained system is expressed as follows: $\mathrm{U(V,\delta)} = \mathrm{U}(V_0, 0) + V_0[\sum_{ij} \tau_i \delta_i \xi_i + 0.5 \sum_{ij} C_{ij} \delta_i \xi_i \delta_j \xi_j]$, where $\mathrm{U}(V_0, 0)$ is the energy of the unstrained system with equilibrium volume V_0, τ_i is an element in the stress tensor, and ξ_i is a factor to take care of Voigt index[22]. For the orthorhombic chalcopyrite compound $SrZrS_3$ has nine independent elastic constants (C_{11}, C_{22}, C_{33}, C_{44}, C_{55}, C_{66}, C_{23}, C_{12}, C_{13}). It requires nine strains to obtain them are summarized in Table 2. Considering the absence of any theoretical and experimental data, the elastic properties obtained in this work should serve as a good reference for further investigation. Meanwhile, according to Born's structural stability criteria, elastic constants in the orthorhombic structure must comply with[23]: $C_{11}+C_{22}-2C_{12}>0$; $C_{11}+C_{33}-2C_{13}>0$; $C_{33}+C_{22}-2C_{23}>0$ and $(\mathrm{C_{11}} + \mathrm{C_{22}} + \mathrm{C_{33}} + 2\mathrm{C_{12}} + 2\mathrm{C_{13}} + 2\mathrm{C_{21}}) > 0$ and $\mathrm{C_{ii}}>0$. From Table 2, it clearly shows that the calculated elastic constants of $SrZrS_3$ with Pnam symmetry satisfy the criteria, which indicates that they are mechanically stable over the pressure range of 0 to 15 GPa.

Table 2. Calculated independent elastic constants for the orthorhombic $SrZrS_3$ compared at zero-pressure.

Pressure	C_{11}	C_{22}	C_{33}	C_{44}	C_{55}	C_{66}	C_{12}	C_{13}	C_{23}
0 GPa	131.3	142.3	97.9	39.5	30.6	43.7	40.9	59.7	43.1
[18]Cal.	137.3	107.4	74.3	32.0	35.4	56.3	44.4	63.6	10.3

Moreover, we investigated the pressure effect of elastic constants of the orthorhombic $SrZrS_3$, as illustrated in Fig. 2. To the best of our knowledge, no experimental and theoretical are available. It can be seen that the elastic constant C_{11}, C_{22}, C_{13}, C_{12}, C_{23}, and C_{55} increase monotonically with the increasing pressure. The elastic constant C_{66} increase firstly and then decrease as pressure increases. However, the elastic constants C_{33} and C_{66} have little change with the increasing pressure. It shows that C_{33} and C_{22} both increase monotonically with pressure increasing. But C_{13} increases slowly at first, then it begins to gradually reduce when the pressure reaches 15 GPa.

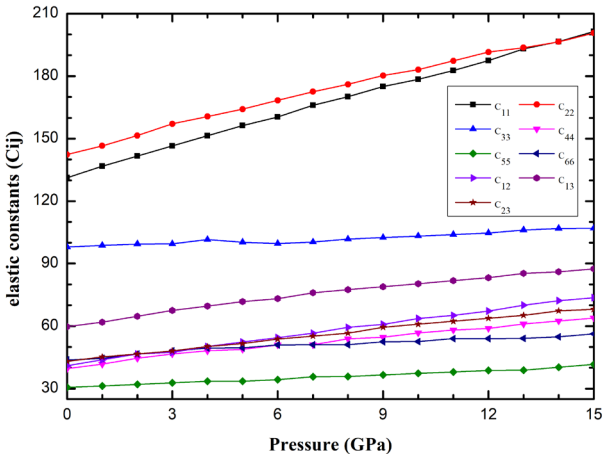

Fig. 2. The elastic constants of the orthorhombic $SrZrS_3$ as functions of pressures.

3.3. Electronic properties

The electronic band structure, partial density of states (PDOS) and total density of states (TDOS) are very important parameters because these parameters help us to understand whether the material will be metallic, semiconducting or insulating[24-25]. To gain more knowledge about physical and bonding characteristics of $SrZrS_3$ compound, the energy band structures were calculated along with specials lines connecting the high symmetry points in the first Brillouin zone. The calculated band structures at 0 and 15 GPa are presented in Fig. 3. The band structure calculations have been carried out following a path along the highest symmetry points G, Z, T, Y, S, X, U, and R. The internal coordinates of these points are (0, 0, 0), (0, 0, 0.5), (-0.5, 0, 0.5), (-0.5, 0, 0), (-0.5, 0.5, 0), (0, 0.5, 0), (0, 0.5, 0.5), and (-0.5, 0.5, 0.5) in the first Brillouin zone, respectively. As can be seen from Fig. 3, the valence band maximum (VBM) and conduction band minimum (CBM) are located at same high symmetry G point.

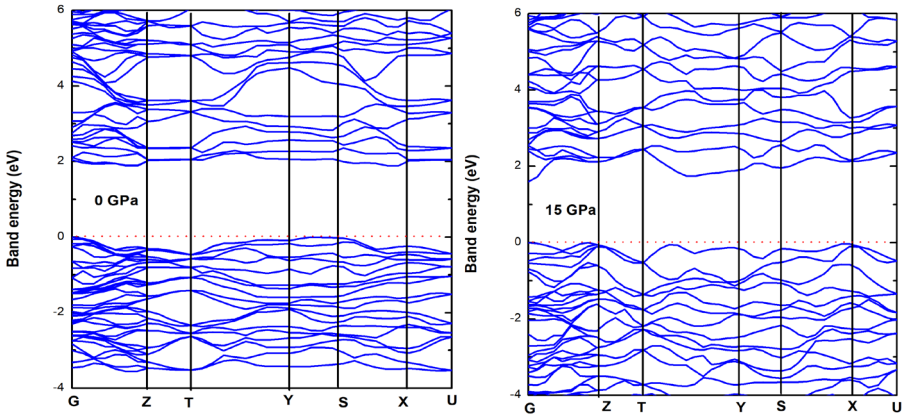

Fig. 3. The band structures of the orthorhombic $SrZrS_3$ at 0 GPa, and 15 GPa, respectively. The red dashed line is marked the Fermi level.

The results indicate that $SrZrS_3$ is a direct band semiconductor with band gap 1.98 eV, which are matched well with experimental data 2.05 eV[17]. Moreover, the total and partial density of states provide more details about the electronic properties of atoms and orbitals. To further elucidate the nature of the electronic band structure, the total density of states (DOS) and partial density of states (PDOS) of $SrZrS_3$ under 0 and 15 GPa are shown in Fig. 4. The states near the valence band top are derived from Zr 3d and S 3p orbitals, and the lowest conduction band is composed of Sr 5s and S 3p orbitals. These results agree with the previous calculation results[18].

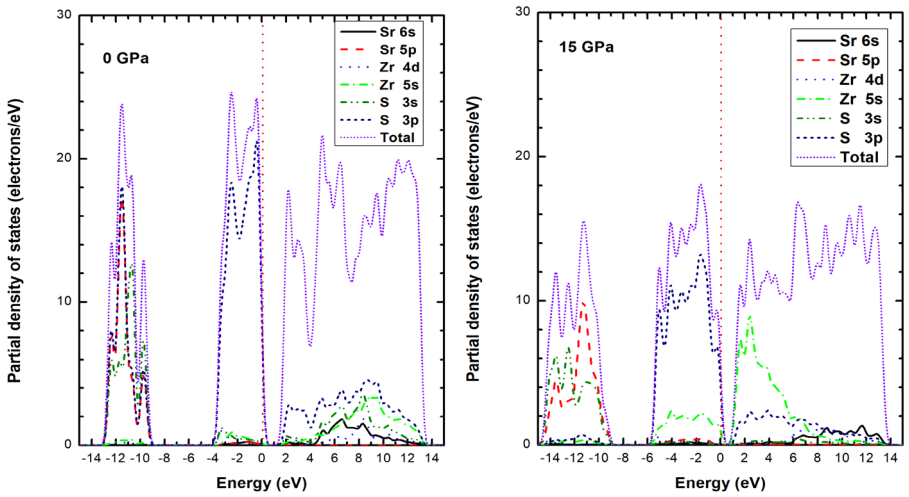

Fig. 4. The density of state (DOS) and partial density of state (PDOS) of $SrZrS_3$ at 0 GPa, and 15 GPa, respectively. The red dashed line is marked the Fermi level.

However, as the pressure increases, the conduction and valence band shift to lower and higher energies, respectively. The shifts of the conduction and valence band result in a decreasing band gap. The pressure dependence of the band gap is shown in Fig. 5, clearly indicating the band gap expend with increasing pressure.

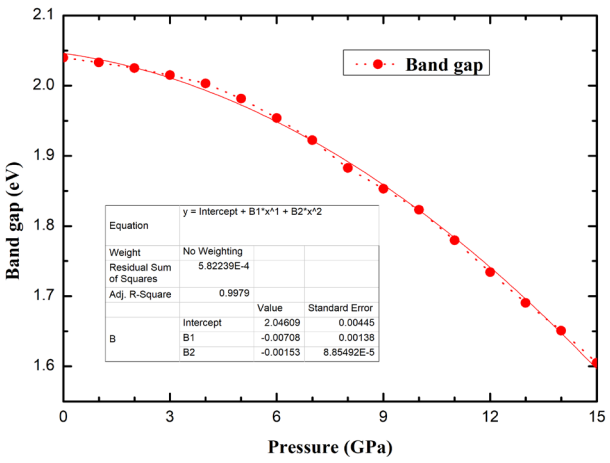

Fig. 5. The band gap of the orthorhombic $SrZrS_3$ under high pressure up to 15 GPa.

To determine the pressure coefficient, we fitted the direct band gap to determine the pressure coefficient, we fitted the direct band gap ($E_g(P)$) with a quadratic function: $E_g(P)=Eg(0)+aP+bP^2$, and obtained a=-0.007 eV/GPa and b=-0.002 eV/$(GPa)^2$. In addition, as the pressure increases, it can be found that the DOS shifts to the higher energies. This result can be explained by the shortened distance between the atoms when compressed, leading to a change in the interaction potentials.

3.4. Optical properties

The optical properties of the orthorhombic $SrZrS_3$ can be obtained from the complex dielectric function $\varepsilon(\omega) = \varepsilon_1(\omega) + i\varepsilon_2(\omega)$, where ω is the angular frequency[26]. The real transition between the occupied and unoccupied electric states commonly depends on the imaginary part $\varepsilon_2(\omega)$. According to the Kramers-Kroning relations, we can derive the real part of the dielectric function. The dielectric function is a crucial physical parameter describing the optical properties, and it reflects the linear response of materials to electromagnetic radiation. The measured real and imaginary parts of dielectric function with varying pressure are shown in Fig. 6(a) and (b). The results from Fig. 6 (a) show that the static dielectric constant $\varepsilon_1(\omega)$ increases from 7.29 to 14.18 when the pressure changes from zero to 15 GPa. Furthermore, the value of $\varepsilon_1(\omega)$ increases from the static value and reaches the main peak, and then it starts to decrease seriously. The values of ε_1 of the main peak are at 10.04 at 2.08 eV, 13.6 at 2.37 eV, and 17.8 at 1.65 eV under a pressure of 0, 10, and 15 GPa, respectively, and the maximum peak value increases with increasing pressure. The highest peak of $\varepsilon_2(\omega)$ represents the strongest absorption of $SrZrS_3$ and drops sharply with the increasing pressure, as shown in Fig. 6 (b). The spectrum shape of ε_2 for the orthorhombic $SrZrS_3$ is almost independent on pressure. The two main peaks of ε_2 are 6.43 at 2.79 eV and 6.96 at 5.51 eV under a pressure of 0 GPa. The main peak of ε_2 shift to lower energy with the pressure increased. For example, with the pressure increases from 10 to 15 GPa, the two peaks at 2.75 eV shift to 2.56 eV and 7.65 eV shift to 7.37 eV. The knowledge of dielectric function helps to calculate all other optical properties such as optical constants. Optical constants are important in designing optical devices.

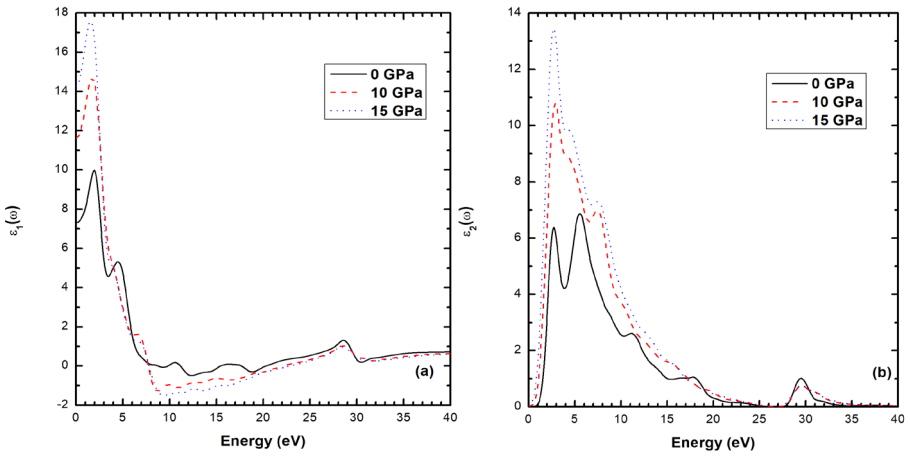

Fig. 6. The dependence of the complex dielectric function of the orthorhombic $SrZrS_3$ at 0 GPa, 10 GPa, and 15 GPa, respectively. (a) the real part $\varepsilon_1(\omega)$ and (b) the imaginary part $\varepsilon_2(\omega)$.

The optical properties of materials can be described by the absorption coefficient, the reflectivity spectrum, the refractive index and the extinction coefficient, and are closed related to dielectric constant. We use the following four formulas: $\alpha(\omega) = \sqrt{2}[\sqrt{\varepsilon_1(\omega)^2 + \varepsilon_2(\omega)^2} - \varepsilon_1(\omega)]^{1/2}$, $R(\omega) = \left|\frac{\sqrt{\varepsilon_1(\omega)+j\varepsilon_2(\omega)}-1}{\sqrt{\varepsilon_1(\omega)+j\varepsilon_2(\omega)}+1}\right|^2$, $n(\omega) = [\sqrt{\varepsilon_1{}^2(\omega) + \varepsilon_2{}^2(\omega)} + \varepsilon_1(\omega)]^{1/2}/\sqrt{2}$, $k(\omega) = [\sqrt{\varepsilon_1{}^2(\omega) + \varepsilon_2{}^2(\omega)} - \varepsilon_1(\omega)]^{1/2}/\sqrt{2}$, to calculate the optical constants: the absorption coefficient ($\alpha(\omega)$), reflectivity ($R(\omega)$), refractive index ($n(\omega)$) and extinction coefficient ($k(\omega)$)[27-28]. Fig. 7 shows the reflectivity ($R(\omega)$), absorption coefficient ($\alpha(\omega)$), refractive index ($n(\omega)$) and the extinction coefficient ($k(\omega)$) at 0, 10, and 15 GPa with photon energy ranging from 0 to 40 eV. The static values of $R(\omega)$ increases from 0.23 to 0.36 when the pressure changes from zero to 15 GPa. From Fig. 7, we can see that peaks of optical constants shift to lower energies with increasing pressure, which meaning undergo a red shift. It is found that, the highest peaks of reflectivity occurred at 19.4, 18.21 and 18.02 eV for 0, 10, and 15 GPa, respectively. Meanwhile, it is worth noting that the absorption edge at 0 GPa is located at 1.68 eV in Fig. 7 (b), which corresponds to the energy band-gap, originating from the electronic transition between the S 3p states at CM and the Zr 5s states at VM. The refractive index and extinction coefficient for the orthorhombic $SrZrS_3$ are shown in Fig. 7 (c) and (d).

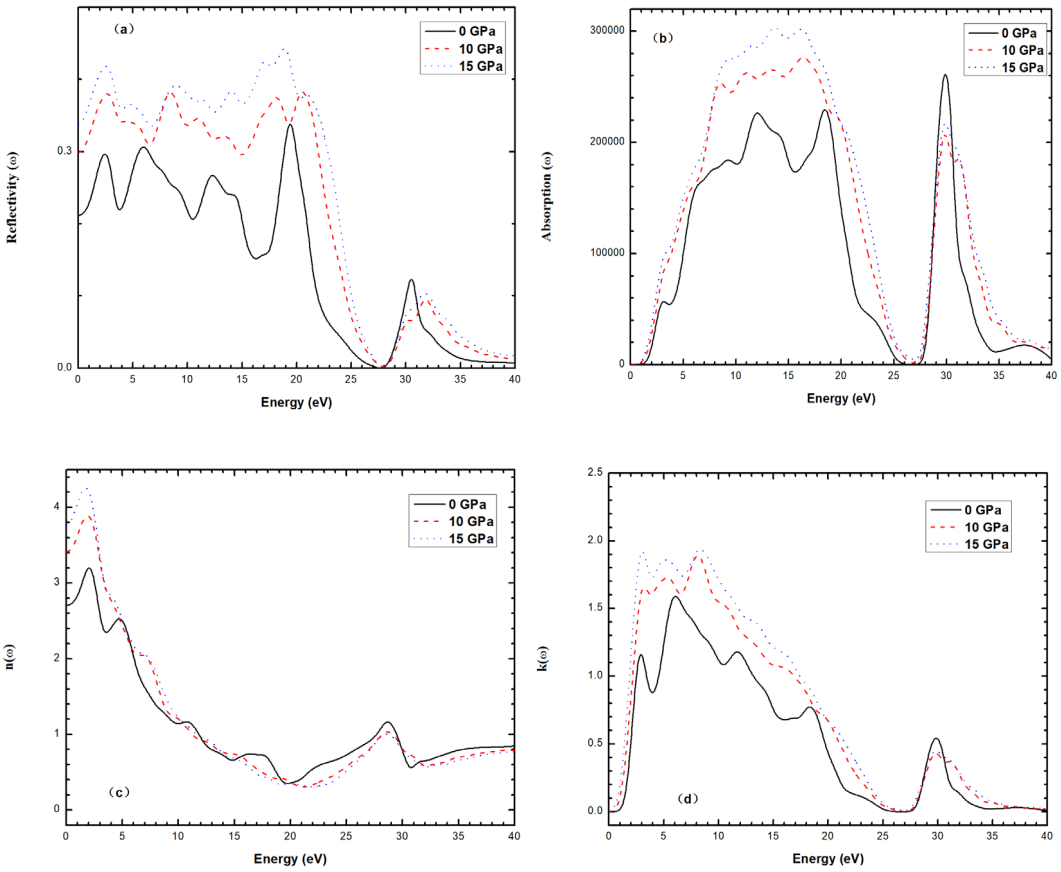

Fig. 7. The optical constants of the orthorhombic $SrZrS_3$ at 0 GPa, 10 GPa, and 15 GPa, respectively. (a) reflectivity ($R(\omega)$); (b) absorption coefficient ($\alpha(\omega)$); (c) the refractive index ($n(\omega)$); and (d) the extinction coefficient ($k(\omega)$).

The static refractive index $n(0)$ of $SrZrS_3$ at 0, 10, and 15 GPa are 2.69, 3.38, and 2.74, respectively. It can be found that the value of $n(0)$ increases with applied pressure. The $n(\omega)$ shows a main peak at around 2.07 eV, 1.84 eV and 2.58 eV for the orthorhombic $SrZrS_3$ at 0, 10, and 15 GPa, respectively. And the $k(\omega)$ shows a main peak at around 6.18 eV, 5.29 eV and 5.28 eV for the orthorhombic $SrZrS_3$ at 0, 10, and 15 GPa, respectively. Both the refractive index and the extinction coefficient shift toward the lower energy region when the pressure increases, which is consistent with absorption coefficient ($\alpha(\omega)$) and reflectivity $R(\omega)$.

4. Conclusion

The crystal structural, electronic, elastic, and optical properties of orthorhombic $SrZrS_3$ was successfully investigated by first-principle calculations. The variation of the structural quantities such as lattice parameters, volume and band gap with increasing pressure does not show any discontinuity up to pressure 15 GPa. Moreover, the pressure dependence of the electronic band structure, the total density of states (DOS) and partial density of states (PDOS) of orthorhombic $SrZrS_3$ were presented. The calculated results show that there is an energy shift both in conduction and valence band which lead to that the band gap decreases smoothly under compression. Meanwhile, according to our work, we found that the optical properties of orthorhombic $SrZrS_3$ undergo a red shift with increasing pressure.

Acknowledgments

This work was supported by Shaanxi College of Communications Technology (group no：2019JQ-541).

References

[1] T. Zhang, M. Yang, Y. Zhao, K. Zhu, Nano Lett. 15, 3959 (2015); https://doi.org/10.1021/acs.nanolett.5b00843

[2] C. Bi, Q. Wang, Y. Shao, Y. Yuan, Z. Xiao, J. Huang, Nat. Commun. 6, 7747 (2015); https://doi.org/10.1038/ncomms8747

[3] W. Nie, H. Tsai, R. Asadpour, J. C. Blancon, A. J. Neukirch, G. Gupta, J. J. Crochet, M. Chhowalla, S. Tretiak, M. A. Alam, H. L. Wang, A. D. Mohite, Science 347, 522 (2015); https://doi.org/10.1126/science.aaa0472

[4] W. Meng, B. Saparov, F. Hong, J. Wang, D. B. Mitzi, and Y. Yan, Chem. Mater. 28, 821 (2016); https://doi.org/10.1021/acs.chemmater.5b04213

[5] W. Yin, T. Shi, Y. Yan, Adv. Mater. 26, 4653 (2014); https://doi.org/10.1002/adma.201306281

[6] H. Brasseur, L. Pauling, J. Am. Chem. Soc. 60, 2886 (1938); https://doi.org/10.1021/ja01279a016

[7] M. Oumertem, D. M. Saadi, N. B. D. P. Rai, R. K. M. Ibrir, J. Comput. Electron. 2, 415

(2019); https://doi.org/10.1007/s10825-019-01317-3

[8] S. Niu, J. M. Guerrero, B. C. Melot, J. Mater. Research. 24, 4135 (2018); https://doi.org/10.1557/jmr.2018.419

[9] M. Ju, J. Dai, L. Ma, X. C. Zeng, Adv. Energy Mater. 8, 2 (2017).

[10] Y. Peng, Q. Sun, H. Chen, W. J. Yin, J. Phys. Chem. Lett. 10, 4566 (2019); https://doi.org/10.1021/acs.jpclett.9b01657

[11] U. Schwarz, F. Wagner, K. Syassen, H. Hillebrecht, Phys. Rev. B: Condens. Matter Mater. Phys. 53, (1996) 12545; https://doi.org/10.1103/PhysRevB.53.12545

[12] M. Szafrański, A. Katrusiak, J. Phys. Chem. Lett. 8, (2017) 2496; https://doi.org/10.1021/acs.jpclett.7b00520

[13] N. D. Mermin, Phys. Rev., 137(5A), A1441 (1965); https://doi.org/10.1103/PhysRev.137.A1441

[14] J. Hafner, J. Comput. Chem., 29(13), 2044 (2008); https://doi.org/10.1002/jcc.21057

[15] J. P. Perdew, A. Zunger, Phys. Rev. B 23, (1981) 5048; https://doi.org/10.1103/PhysRevB.23.5048

[16] H. J. Monkhorst, J. D. Pack, Phys. Rev. B. 3, 5188 (1976); https://doi.org/10.1103/PhysRevB.13.5188

[17] C. S. Lee, K. M. Kleinke, H. Kleinke, Solid State Sci. 7, 1049 (2005); https://doi.org/10.1016/j.solidstatesciences.2005.02.010

[18] H. I. Eya, E. Ntsoenzok, N. Y. Dzade, Mater. 13, 978(2020); https://doi.org/10.3390/ma13040978

[19] M. Ishii and M. Saeki, Phys. Status Solidi B 170, K49 (1992); https://doi.org/10.1002/pssb.2221700149

[20] M. Ishii, M. Saeki, and M. Sekita, Mater. Res. Bull. 28, 493 (1993); https://doi.org/10.1016/0025-5408(93)90132-W

[21] P. Vinet, J. R. Smith, J. Ferrante, J. H. Rose, J. Phys. C 19, L467 (1986); https://doi.org/10.1088/0022-3719/19/20/001

[22] L. Fast, J. M. Wills, B. Johansson, O. Eriksson, Phys. Rev. B. 51, 17431 (1995); https://doi.org/10.1103/PhysRevB.51.17431

[23] Z. J. Wu, X. F. Hao, X. J. Liu, J. Meng, Phys. Rev. B. 75, 054115 (2007).

[24] R. Devanathan, N. Yu, K. E. Sickafus, M. Nastasi, J. Nucl. Mater. 232, 59 (1996); https://doi.org/10.1016/0022-3115(96)00388-1

[25] T. Isobe, K. Daimon, T. Matsubara, Y. Hikichi, .Ceram. Int. 33, 1211 (2007); https://doi.org/10.1016/j.ceramint.2006.03.027

[26] A. H. Reshak, S. Auluck, Phys. Rev. B. 68, 125101 (2003); https://doi.org/10.1103/PhysRevB.68.125101

[27] Y. Matsumoto, J. Solid State Chem. 126, 227 (1996); https://doi.org/10.1006/jssc.1996.0333

[28] R. Devanathan, N. Yu, K. E. Sickafus, M. Nastasi, J. Nucl. Mater. 232, 59 (1996); https://doi.org/10.1016/0022-3115(96)00388-1